RASĀYAN *J. Chem.*
Vol. 19 | No. 4 | 2001-2013 | October-December | 2026
ISSN: 0974-1496 | e-ISSN: 0976-0083 | CODEN: RJCABP
http://www.rasayanjournal.com
http://www.rasayanjournal.co.in

ZnO-NiO NANOCOMPOSITES SYNTHESIZED VIA A FACILE SONOCHEMICAL ROUTE FOR HIGH-PERFORMANCE PHOTOCATALYTIC AND ELECTROCHEMICAL SENSING APPLICATIONS

Sharanakumar T.M.[1,✉], S. Soundeswaran[2], G. Srinivas Reddy[3], Puneeth Kumar N.[4], T. Naveen Kumar[5], K. M. Mamatha[2], M.N. Somashekar[6], and C.R. Ravikumar[7]

[1]Department of Chemistry, Ballari Institute of Technology and Management, Jnana Gangotri Campus, Ballari-583104, Karnataka, India
[2]Department of Chemistry, Dr. Ambedkar Institute of Technology, Bangalore-560078, Karnataka, India
[3]Department of Physics & Chemistry, Mahatma Gandhi Institute of Technology, Hyderabad-500075, Telangana
[4]Department of Mechanical Engineering, CMR Institute of Technology, Bangalore-560037, India
[5]Department of PG Chemistry, Surana College, Autonomous Institute, Bangalore, India
[6]HKE Society's Sree Veerendra Patil Degree College of Science, Arts & Commerce, Sadashivanagar, Bengaluru-560080
[7]Research Centre, Department of Chemistry, East-West Institute of Technology, VTU, Bangalore-560091, India
✉Corresponding author: sharanbkl99@gmail.com

ABSTRACT

Tulsi leaf extract was used in a sonochemical process to produce the Zn: NiONC. Several spectral techniques were used to study the composite material. Zn: NiONC crystallites of a size of 28 nm are visible in XRD. The SEM reveals a hexagon-shaped particle with an average particle size of about 80 nm. The DRS spectra show that the energy band-gap value of Zn: NiO NC is 3.223 eV. The NC PCA was evaluated using Congo Red dye photodegradation; the results show that under UV-Vis light, the highest absorption was seen at 497 nm with 80.9% degradation. The Zn: NiONC is also used as an electrode in CV studies. In a 1 M HCl solution, it shows the surface redox process of Ni^{2+} to Ni^{3+} at 0.31 V and 0.15 V at 10 mV/s. By exhibiting a redox peak in the CV spectrum, the Zn: NiONC successfully identified lithium. This suggests that the electrode is suitable for use as a sensor electrode.

Keywords: Zn:NiO NC; CR dye; Photocatalytic Activity; Electrochemical sensor; Lithium.

RASĀYAN*J. Chem.*, Vol. 19, No.4, 2026

INTRODUCTION

The control, monitoring, and removal of some industrial pollutants have become essential due to their release into the aquatic environment. These pollutants include paint, medicines, textiles, leather, food, and many other harmful items. These contaminants affect the entire biota and cause a number of diseases due to their non-biodegradable nature. To establish a safe and healthy environment, organic effluents must be removed.[1] Photocatalysis has gained appeal in recent decades, especially as a solution to energy and pollution problems. Its objective is to develop a low-cost, ecologically friendly catalyst with adequate mineralisation potential.[2,3]

The mineralisation process has relatively limited uses since the bandgap of the several semiconductors usually prevents it. To create new kinds of photocatalysts that show notable activity when exposed to UV light, it is therefore important to alter the semiconductors. Numerous metal oxides, including TiO_2, Co_3O_4, Ag_2O, ZnO, and NiO, have been employed for the photochemical mineralisation of hazardous compounds

http://doi.org/10.31788/RJC.2026.1949958

during the last few decades.[4-6] However, there are several serious disadvantages to all of these photocatalysts, including (i) aggregation of nanoparticles, (ii) decreased light transmittance, and (iii) decreased surface area. Consequently, more innovative synthesis is required to enhance photocatalytic efficiency. Organic dye pollution predominantly affects the brain, liver, and central nervous system in humans due to its long-term toxicity and lack of biodegradability.[7] Therefore, wastewater effluents containing dyes must be treated immediately before being released into the atmosphere. Congo Red (CR) is a synthetic dye commonly utilised in textiles and biological staining, particularly in histology.[8] Among many azo dyes, it is well renowned for its vibrant colour and ability to stick to a wide range of surfaces. Nevertheless, CR and related dyes can cause environmental issues because of their longevity in soil and water systems, which makes their degradation a major concern. When dyes like CR are disposed of incorrectly, they can contaminate water, damage aquatic life, and perhaps cause harm to humans because of their breakdown components that cause cancer.[8]

Therefore, the development of effective degradation strategies is necessary to reduce their environmental impact. The numerous technology perspectives are being used to study the vast field of nanoscience. Over the past few decades, research has concentrated on nanocomposite (NC) materials because they combine unique features. These days, more thought is being paid to supercapacitors and batteries when creating novel solutions to energy-related issues.[9,10] Since nanocomposites combine the characteristics of their component materials, they are the subject of extensive research in the fields of energy and catalysis. High band-gap energy (Eg) semiconductors with unique traits, such as TiO_2, NiO, ZnO, SnO_2, etc., are currently gaining more attention because of their many applications.[11,12] Piezoelectric devices, photocatalysis, LEDs, Emission control, hybrid solar cells, gas-sensing devices, UV shields, temperature control paints, and supercapacitors are just a few of the many applications for metal oxide (MO) semiconductors.[13-21] Increased use of semiconductor materials is necessary to repair our damaged atmosphere and promote sustainable technological advancement. The evolution of sophisticated electronic traits that are useful and satisfying is required by the growth of electronic basis technologies.[22] The supercapacitor and sensor are efficient energy-storage components for high-power-demand applications in next-generation energy-storing systems.[23] In recent years, metal nanostructures have been the subject of extensive research.

Specifically, metal nanoparticles (NPs) combined with oxide systems have attracted attention owing to their potential in a variety of fields, such as biomedical research, photocatalysis, sensing, catalysis in different transformations, supercapacitors, etc.[24,25] NiO is a crucial metal oxide with numerous uses because of its advantageous qualities, comprising fuel cell composite anodes, energy storage systems, dye-sensitized photocathodes, gas sensing, smart windows, solar cells, electrochromic coatings, and supercapacitors.[26,27] It is a widely recognised semiconductor material with a vast band gap that has catalytic, electrical, and optical properties.[28] The high theoretical capacitance (2584 F/g for NiO), low cost and environmental friendliness, good chemical and thermal stability, availability of supply, and other characteristics make nickel-based materials interesting as electrode materials.[29] However, NiO's low intrinsic conductivity, poor reaction kinetics, and small number of electrochemically active sites restrict its potential for pseudocapacitance; only the near-surface area does.[30] Therefore, it would be beneficial to investigate conductivity augmentation alternatives to have a good understanding of the functional capabilities of NiO with NC structures. Zinc nanoparticles have numerous scientific and economic uses, but they are also gaining popularity because of their special chemical, physical, and biological characteristics, like their higher electrical conductivity.[31,32] Additionally, research has shown that Zn nanostructures have remarkable catalytic properties for the reduction of organic pigments.[33,34] Due to their effectiveness and affordability, ZnNPs have been thoroughly investigated as a catalyst in industrial applications.[35] There have also been reports of studies on Zn NPs improving the electrochemical stability of electrode materials.[36] The previous study examined the effects of Zn loading on graphene-based nanocomposites' supercapacitor performance.[37] Investigating the catalytic and electrochemical characteristics of Zn-incorporated NiO systems would be intriguing. We have chosen Zn-NiO (zinc-nickel oxide) composites for the present study's photocatalytic and sensor applications due to their superior photocatalytic and sensor capabilities over their individual components. Zn and NiO both boost photocatalysis and sensor efficiency by combining their own benefits.[38,39]

Since NiO is a p-type semiconductor with a broad band gap (~3.4–4.0 eV), it mostly absorbs light in the ultraviolet spectrum.[38,39] Its high electron-hole pair recombination rate, however, restricts its photocatalytic activity. ZnO's high electron mobility and resistance to photocorrosion make it a semiconductor with a broad bandgap (3.2 eV) that exhibits good photocatalytic characteristics under UV light. ZnO and NiO combine to form a hetero junction, which enhances charge separation and increases light absorption in the nanocomposite.

The overall photocatalytic efficiency is increased as a result. Due to the combination of strong electrical conductivity from Zn and high pseudocapacitive behaviour from NiO, the Zn: NiO NC has potential performance as a material for supercapacitors and sensors.[40] By incorporating the advantages of both elements, this hybrid construction improves electrochemical performance. Because of redox reactions on its surface, NiO is distinguished for having exceptional pseudocapacitive qualities. High specific capacitance can result from reversible Faradaic processes in NiO, which include charge transfer. By offering effective electron routes, Ag nanoparticles improve the composite's conductivity, which raises the total rates of discharge and charge storage. This combination raises the composite's specific capacitance.[41] NiO's performance in supercapacitors may be constrained by its low intrinsic electrical conductivity.

Nevertheless, the composite's electrical conductivity is greatly enhanced by the addition of Ag nanoparticles. By acting as a conductive network, zinc lowers internal resistance and accelerates electron movement during discharging and charging. Higher charge storage capacity is the outcome of NiO and Zn's synergistic interaction.[42] The composite structure's wide surface area, great electrochemical activity of NiO, and high optimum conductivity of Zn result in faster ion/electron transit and better usage of active materials.[43] In our work, we used tulsi leaf extract and a sonochemical approach to produce Zn: NiONC. Several spectroscopic techniques were used to study the composite material. Zn: NiONC crystallites have an average size of 28 nm, according to XRD. The SEM image shows a hexagonal shape.

The TEM images show that NiO exhibits diffraction rings and spots consistent with its cubic structure, while Zn diffraction spots often match the hexagonal structure. The energy band gap value of Zn: NiONC is 3.223 eV, according to the DRS spectra. The Congo Red (CR) dye photodegradation was used to assess the NC Photocatalytic Activity (PCA). The results indicate that, under UV light irradiation, maximum absorption was seen at 497 nm with 80.9% degradation with respect to time. CV investigations also employed Zn: NiONC as an electrode. The surface redox process of Li to Li^+ is demonstrated in a 1 M HCl solution at 0.31 V (cathodic) and 0.15 V (anodic) at 10 mV/s. The Zn: NiONC effectively detected lithium by showing a redox peak in the CV spectra. This implies that the electrode can be used as a sensor device.

EXPERIMENTAL

Materials and Methods

Analytical reagent (A.R.) is used by Sigma-Aldrich to extract every chemical. NaOH, Congo Red, 0.1 M HCl, double-distilled water, nickel nitrate ($Ni(NO_3)_2.6H_2O$), and zinc nitrate ($Zn(NO_3)_2.6H_2O$) are some of these. For the CV investigations, three electrode systems were employed: Ag-AgCl served as the reference electrode, platinum served as the counter electrode, and prepared NC served as the working electrode.

Preparation of Zn: NiONC

Zn: NiONC was produced using the sonication process (ultrasound radiation method). The primary precursors were 1.1 ratios of nickel nitrate hexahydrate ($Ni(NO_3)_2.6H_2O$) and 1 M zinc nitrate hexahydrate ($Zn(NO_3)_2.6H_2O$). Next, gently mix the liquid above while adding 1 M sodium hydroxide (NaOH) dropwise. A microprocessor-controlled 13 mm-diameter ultrasonic probe made of premium titanium alloy (model PRO-550, 20 kHz, 500 W) operating at 20% amplitude, 20 kHz frequency, and potentially dissipating 100 W of power was used to expose this solution to high-intensity ultrasound radiation for two hours at 45 °C.[44] A brown precipitate was produced when the reaction was complete. After centrifuging the mixture to eliminate any leftover NaOH, the precipitate was washed with ethanol and distilled water. Following an hour of drying at 100 °C in a hot air oven, the precipitate was calcined for three hours at 400 °C to generate brown Zn: NiONC (Scheme-1).

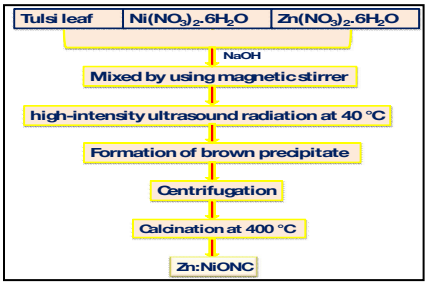

Scheme-1: Schematic Route for the Synthesis of Zn: NiONC

Photocatalytic Activity

To test the synthetic material's capacity to promote photocatalytic degradation, we selected an industrial dye known as CR dye. The photocatalyst and the dye molecules were continually mixed in the dark during this phase to stabilise any physical dye adsorption onto the catalyst surface before irradiation. Achieving this equilibrium suggests that the subsequent decrease in dye concentration after light exposure is solely due to photocatalytic breakdown rather than ongoing adsorption. The catalyst and dye solution were first put in a container and stirred with a magnetic stirrer for 130 minutes in the dark. This stage was crucial to bringing the system to balance. A 125 W mercury vapour lamp was used as the UV light source for the irradiation. This light was placed inside a 176 cm^2 circular glass reactor, 21 cm away from the dye solution. A stock solution of the dye was initially made in a 250 mL standard flask in order to create a 10 ppm solution. Additionally, the catalyst concentrations in the solution were changed, starting at 20 mg. To make sure that any nanoparticles were removed, a 5 mL sample of the solution was taken during the UV irradiation approach and passed through a filtration process at regular intervals of 15 minutes. The filtered solution was then examined using the Shimadzu UV-Vis spectrometer, which operated in the wavelength range of 200 to 800 nm, to ascertain the extent of deterioration.[43]

Working Electrode Preparation

Graphite powder, produced NC, and binder (PTFE) were mixed in an agitated mortar in a 70:15:15% ratio to create the working electrode. A nickel mesh was compressed for six minutes at 25 MPa after being coated with an active material to increase electrical conductivity. To improve the electrolytic mobility, the built electrode was submerged in a 0.1 N HCl solution for 20 minutes.[46]

RESULTS AND DISCUSSION

Characterization Techniques

An effective non-destructive analytical method for examining the orientation, phase composition, and crystal structure of liquid, solid, and powdered materials is X-ray diffraction (XRD). The formation of cubic crystal NiO was confirmed by the XRD pattern, which displays five distinct peaks at 2θ values of 37.13^O, 43.15^O, 62.63^O, 75.22^O, and 79.09^O. These peaks are identified as reflection peaks from planes (111), (200), (220), (311), and (222) (JCPDS card no. 00-087-0719). Fig.-1(a). Furthermore, peaks other than the NiO are shown in Fig.-1(a) that correspond to the hexagonal Zn planes (100), (002), (101), (102), (110), (200), (112), and (201) (JCPDS card no. 00-089-1397). The crystalline quality of the Zn: NiONC validated both XRD peaks, and no other peaks were generated apart from the NiO and Zn. The synthesised Zn: NiONC was successfully confirmed by the results. The average crystallite size of the Zn: NiONC was calculated using the Scherrer formula.[42,47] Zn: NiONC crystallites are about 28 nm in size on average. SEM studies was used to look at the surface morphology, physical properties, and Zn distribution over the NiO surface.

As seen in Fig.1(b), NiO surfaces have a porous flower-like shape, and adding Zn to its pores does not significantly change the material's morphology. NiO nanostructures were shown to have a cubic form and an average particle size of roughly 80 nm in the SEM image in Fig.-1(b). These are Zn and NiO compositions, as the preceding result demonstrates. The EDAX method was used to determine a sample's chemical constituents. The presence of Zn (37.5%) and the necessary elements Ni (39%), C (6.7%), and O (16.8%) in the modified NiO nanoparticle is confirmed by Fig.-1(c). The existence of Zn throughout the surface of the desired NiO structure is fully supported by the appearance of several signals

corresponding to these elements. The elemental mapping for O, C, Ni, and Zn in Fig.-1(c) indicates the presence of the corresponding Zn.[48]

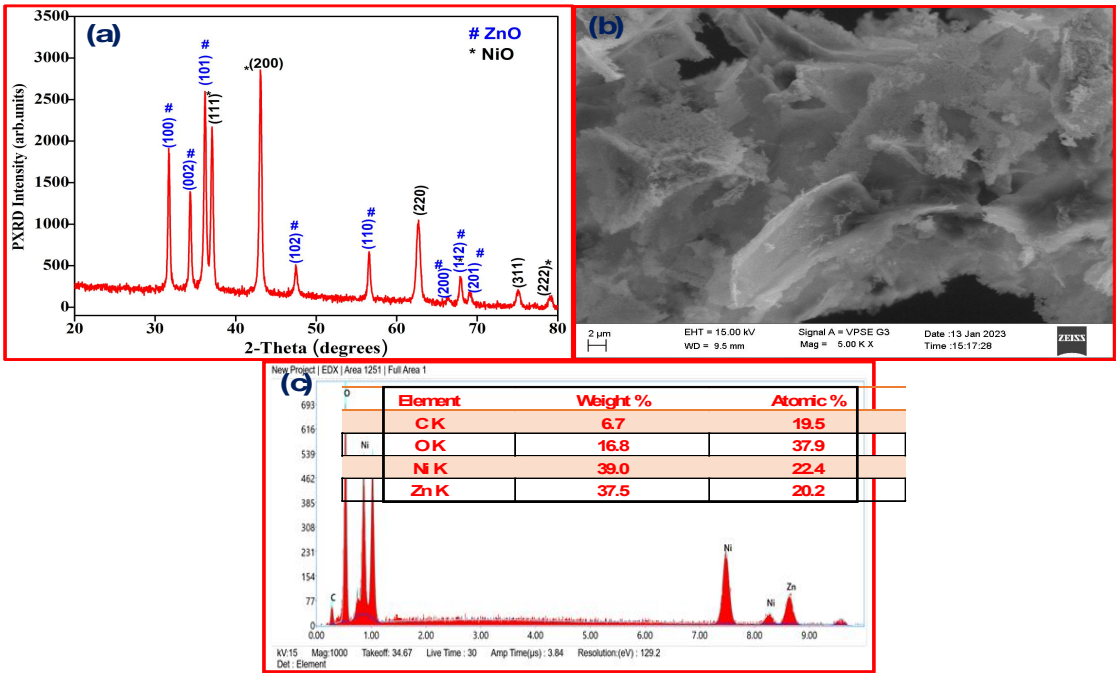

Fig.-1: (a) XRD Spectral Data of Zn: NiONC (b) SEM Image of Zn: NiONC (c) EDAX Analysis of Zn: NiONC

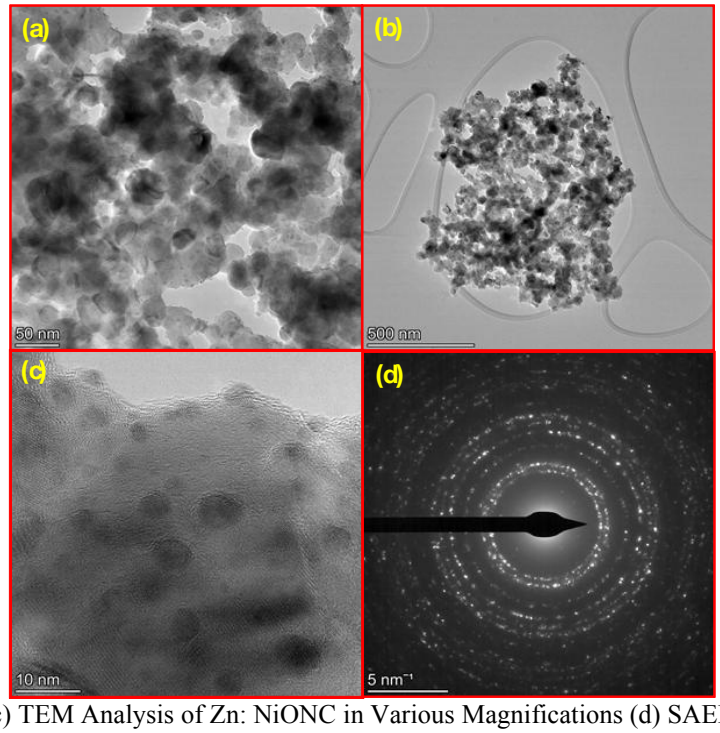

Fig.-2: (a-c) TEM Analysis of Zn: NiONC in Various Magnifications (d) SAED Spectral Analysis

The structural morphology of the Zn: NiONC materials was deeply understood by the use of TEM. Three phases, namely NiO and Zn, were confirmed by the TEM picture in Fig.-2(a to c) at 10 nm, 50 nm, and 500 nm magnifications. The structures revealed were face-centred cubic and hexagonal. TEM image in Fig.-2 (a-b) shows lattice fringes with a spacing of 0.22 to 0.26 nm, which correspond to the (200) and (101) planes of Zn and NiO, respectively.[49] The microscopic results, which are in good alignment with

the XRD data, validate the synthesis of Zn: NiO NC. The highly agglomerated particle structure, a feature of combustion-produced materials, is clearly seen in the TEM image. A distinctive ring in Fig.-2(c) characterises the SAED pattern. The crystalline character of the Zn and NiO phases is confirmed by the diffraction spots or rings that correspond to them. While Zn diffraction spots typically fit the hexagonal structure, NiO shows diffraction rings and spots that are consistent with its hexagonal structure.

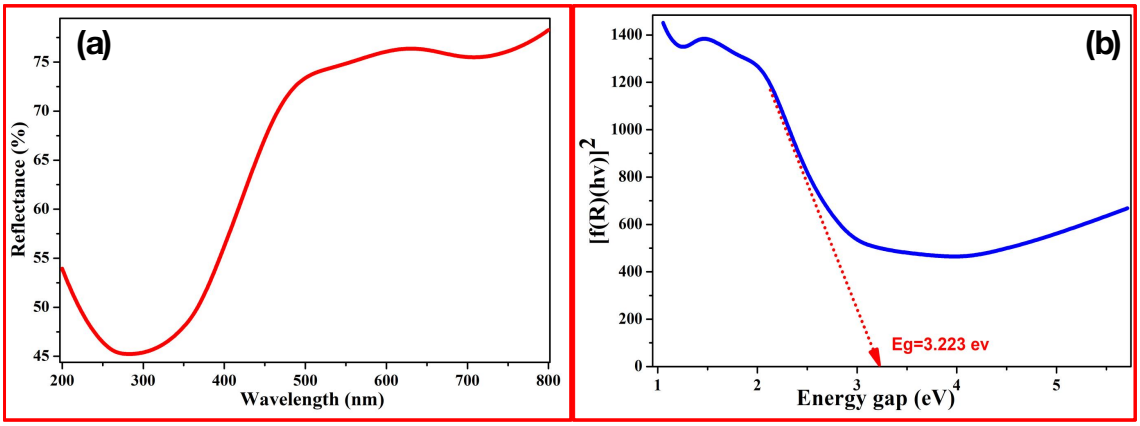

Fig.-3: (a) UV Spectra of Zn: NiONC (b) Energy Bandgap of Zn: NiONC

Zn: NiONC absorbance in the UV region is shown in the Fig.-3(a). Equation (1) is used for calculate the energy band gap.

$$E=\frac{hc}{\lambda} \qquad (1)$$

The UV spectra show that the Zn: NiO NC has a band-gap value of 3.223 eV, which is consistent with earlier studies on the substance[49,50] Fig.-3(b). These features were shown to be caused by the interfacial electrical interaction between Zn and NiO in Zn: NiO NC via O 2p, which raises the valence band potential through electron-electron repulsion and decreases the band gap.[49,50]

PCA of Congo Red dye

The photocatalytic activity of Zn: NiONC was measured using an anionic organic dye. The photodegradation of CR dye was investigated using the Zn: NiONC PCA for a duration of 0 to 120 minutes. The UV region's maximum absorption was measured at 497 nm (Fig.-4(a)).[51] Figure-4(a) unequivocally demonstrates that the absorption peak value falls as the time period enhances, confirming the degradation of the CR dye under UV light. Figure-4(b) shows that the percentage of deterioration rises from 0 to 120 minutes after UV exposure. The photodegradation rate of the CR dye rose to 80.9% when exposed to UV radiation. It shows that when exposed to UV light, Zn: NiONC has higher PCA as a catalyst in the degradation of CR dye.

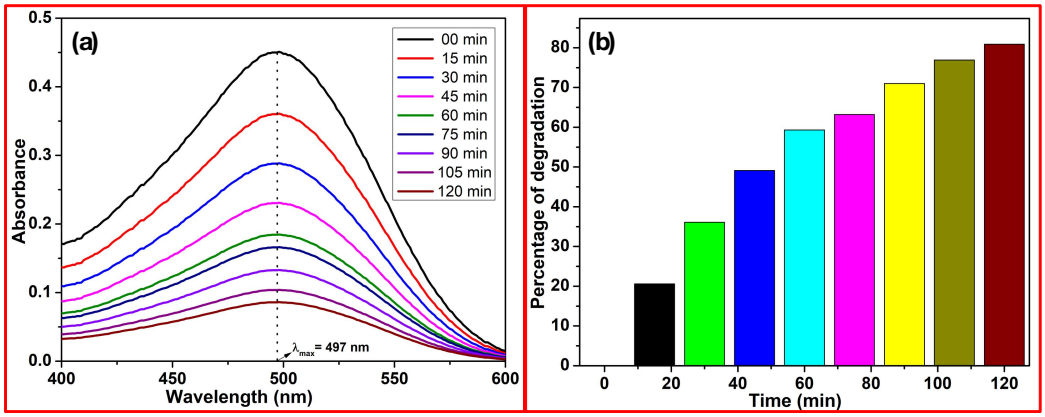

Fig.-4:(a) Photocatalytic Deterioration of CR Dye under UV Light Irradiation (b) Percentage of Degradation v/s Time

Kinetic Studies

50 millilitres of dye solution, starting at 2.2×10^{-3} mol. The impact of Zn: NiONC kinetics was measured using the pseudo-first-order equation.[52] After 120 minutes of UV light exposure, the Zn: NiONC's PCA gradually increased. According to the C/Co equilibrium values, NiO had a significantly lower C/Co value than Zn: NiO, indicating that the inclusion of zinc dopants enhanced photocatalytic performance (Fig.-5(a and b)). Previous research indicates that higher photocatalytic activity is correlated with reduced optical band gap energy.[51,52] In this study, the band gap lowering improved the electrical interaction between the dye molecules and NiO.

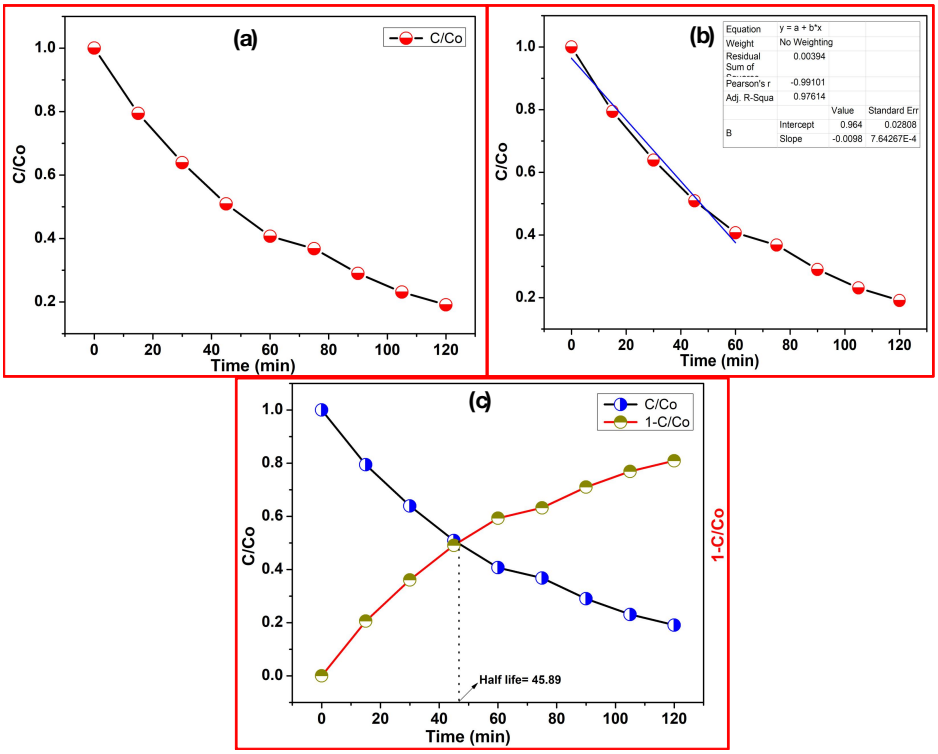

Fig.-5: (a & b) Kinetic Studies of Zn: NiONC, (c) the Plot of Pseudo First-Order Kinetics of Zn: NiO NC

A narrower band gap enhanced charge transfer from the valence band to the conduction band, facilitating charge transfer from the catalyst to the dye molecules' Fermi level. Dye molecule adsorption increased on the catalyst's surface as a result, increasing the degradation efficiency.[52] The results demonstrate that adding Zn dopant to NiO thin films has a considerable impact on the photocatalytic breakdown of CR. During CR degradation, the k app values rise in a direct relationship to the Zn dopant level. This suggests that Zn increases PCA in the NiO lattice, which speeds up degradation.[45] Zn ions increase the production of reactive oxidative species and accelerate the breakdown of CR by creating more electron and/or hole trapping sites. The photocatalytic efficiency of Zn: NiONC catalysts is evaluated by measuring CR dye degradation. In Fig.-5(b), a plot of C/Co v/s time, the pseudo-first-order kinetics of the degradation process were displayed as a straight line. Based on the graph's slope, a rate constant (k_1) of 0.01359 min^{-1} (R_2 = 0.9761) for CR dye was determined. As shown in Fig.-5(c), the concentration of CR dye (C/Co) clearly drops as the irradiation period rises. After 120 minutes of photoirradiation, the CR dye concentrations decreased from 1.0 to 0.19, with a half-life of 45.89 for Zn: NiONC.

Mechanism

A schematic of the Congo Red dye degradation process is seen in Fig.-6. When exposed to UV light, Zn: NiONC generates electrons at the valence band (VB) and holes at the conduction band (CB), respectively. The addition of •OH and/or •NO_2, which breaks down the azo group (-N=N–, CR's chromophore) and creates hydroxylation products, may be the main reason why CR decolourises. The photocatalytic degradation mechanism of Congo red dye can be summed up using Equations-2 to 9.[53]

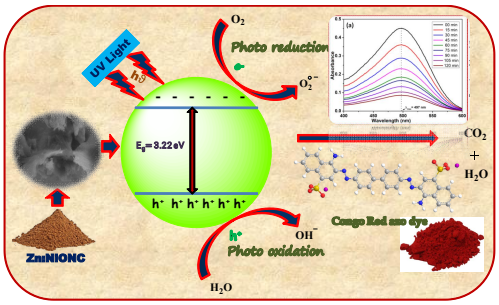

Fig.-6: Photocatalytic Degradation Mechanism of Congo Red Dye

$$Zn{:}NiO + h\vartheta \longrightarrow Zn{:}NiO + e^- + h^+ \quad (2)$$

$$h^+ + H_2O \longrightarrow OH + H^+ \quad (3)$$

$$h^+ + OH^{\bullet} \longrightarrow OH \quad (4)$$

$$e^- + O_2 \longrightarrow O_2^- \quad (5)$$

$$O_2^- + H^+ \longrightarrow HO_2 \quad (6)$$

$$2e^- + HO_2 + H^+ \longrightarrow OH + OH^- \quad (7)$$

$$O_2^- + \text{Congo red dye} \longrightarrow \text{Degraded product} \quad (8)$$

$$e^- + \text{Congo red dye} \longrightarrow \text{Degraded product} \quad (9)$$

Electrochemical Detection of the Zn: NiONC/CPE for Lithium

Investigating their electrocatalytic reaction is made possible by the intriguing characteristics of Zn: NiONC with reference to the electrochemical detection of Li on Zn: NiONC/Carbon paste electrode (CPE). The potential window of 0.4 V to -0.8 V and the CVs of 1 µM lithium on the bare CPE at a scan rate of 50 mVs^{-1} are displayed in Fig.-7. The exceptional redox behaviour of lithium indicated Zn: NiONC's exceptional electrocatalytic activity and high surface-to-volume ratio when it was applied to the electrode surface. However, the addition of 1 µM Li causes a notable increase in the current response and two distinct redox peaks: an anodic peak at 0.15 V and a cathodic peak at 0.31 V (Fig.-7(a)). These results indicate that the electrochemical properties of the modified electrode are substantially improved by the Tulasi leaf-assisted Zn: NiONC. The Zn could be caused by the CP electrode's increased surface energy, large accessible surface area, and improved electron transfer reaction. The electrochemical characteristics of the modified electrode were found to be improved by NiONCs.[54]

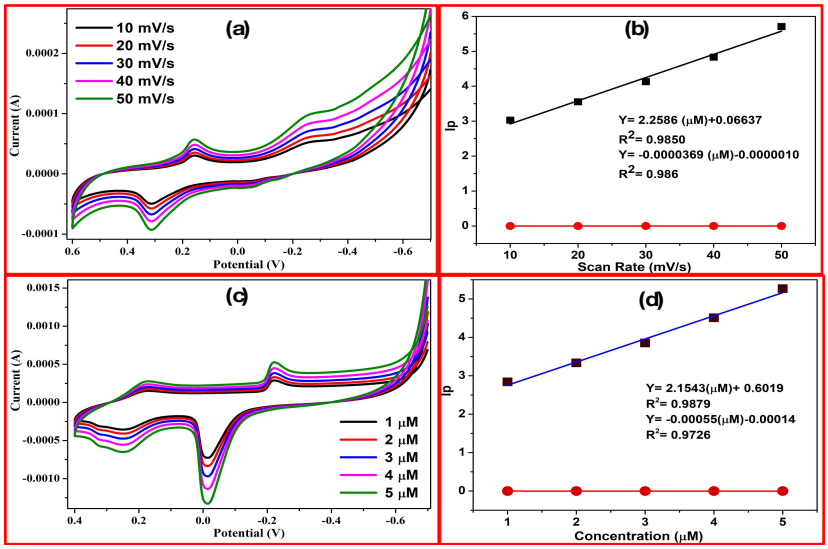

Fig.-7: (a) CVs of the Zn: NiONC Electrode and how the Scan Rate Varies. (b) Calibration Curve (c) CV Analyses of the Zn: NiONC Electrode and Changes in the Concentration of Lithium. (d) Calibration Curve

The Zn: NiONC/CPE electrochemical response at 10 mV/s as a function of scan rate is shown in Fig.-7(a). The oxidation peak current vs. square root of scan rate calibration plots in Fig.-7(a) show linearity with regard to different scan rates on the modified electrode. The redox peak currents directly correlated with an increase in scan rate from 10 to 50 mV s^{-1}. Furthermore, the oxidation and reduction peak potentials changed more favourably and unfavourably, respectively. The anodic peak current correlation coefficients of -0.22 V and -0.013 V demonstrate that diffusion mechanisms control the general dynamics[55]. Within the designated scan rate range, the oxidation peak current correlated linearly with the square root of the scan rate, and as the scan rate increased, the peak separation grew. Furthermore, as evidenced by the minimal change in the potential difference between the oxidation and reduction peak currents, the Zn: NiONC/CPE showed enhanced electrochemical activity. Depending on the electrolyte and electrode material, lithium typically exhibits significant redox properties in CV. At a negative voltage, lithium easily oxidises (loses an electron) to form the lithium ion (Li^+). It can be reduced back to metallic lithium at the same voltage after going through a highly reversible redox process during the reverse scan, which is usually indicated by a noticeable peak in the CV. Peak current against voltage is plotted on a graph, and the linear calibration equation and linear regression curve are displayed in (insert Fig.-7(b)). The CV method's excellent current sensitivity and precision allow for the measurement of Zn: NiONC electrocatalytic activity. The CV tests in 0.1N HCl with different concentrations of Li (1 µM to 5 µM) further demonstrated that the green-produced Zn: NiONC behaved well electrochemically for Li detection, as seen in Fig.-7(c). The outcome showed that the electrocatalytic response of the modified electrode for Li detection is highly concentration sensitive[56], as the Ipa current steadily rose as the concentration of Li in the HCl increased. This kind of instantaneous electrode response shows that Li's redox activity is effectively stimulated by the material (Zn: NiONC) to generate the distinctive voltammetric signals. The graph in (Fig.-7(d)) plots the linear regression curve and linear calibration equation against peak current versus concentration.

Impedance Spectra

Figure-8 displays the Zn: NiONC impedance data's Nyquist plot. The y-axis represents the imaginary component, while the x-axis represents the real component. The Nyquist plot can be divided into two parts based on frequency: (i) a semicircle-shaped high-frequency zone that illustrates charge transport at the electrode–electrolyte interface; and (ii) a low-frequency region that displays the electrode capacitance and is represented by a straight line. The diameter of the semicircle arc on the real axis can be rapidly ascertained using charge-transfer resistance (RCt), capacitance (Cdl), and equivalent circuit fit data. The exceptionally low RCt and Cdl of Zn: NiONC are found to be 42.5 °C and 0.000143 F, respectively. This implies that Zn: NiONC's charge transfer mechanism is highly effective, enabling rapid and effective energy transfer.

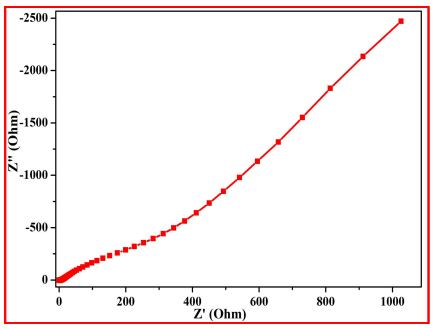

Fig.-8: Impedance Spectra of Zn: NiONC

Zn: NiONC's low resistance demonstrates strong conductivity and efficient charge transfer between its constituents. Further investigation into this Rct engaged in the sensing activity is required to ensure that the Zn: NiONC system functions as efficiently as possible.[57]Zn: NiONC stability tests were carried out by 5 µM lithium in the CV for 10 cycles. The peak potential (Epa) and peak current (Ipa) do not change during the cycle's repetition. The formula to obtain the Zn is Ipn / Ip1: proportion of NiONC disintegration[58,59], where Ipn and Ip1 are the peak current levels for the n^{th} and 1^{st} cycles, respectively.

This results in 94.44%, demonstrating Zn: NiONC's remarkable stability and functioning even after ten cycles.

CONCLUSION

In this study, we were able to successfully synthesise Zn: NiONC using a sonochemical method and extract it from Tulsi leaves. Several spectral approaches were used to study the composite material. The average size of Zn: NiONC crystallites is revealed by XRD to be around 28 nm. The SEM picture displays a hexagonal shape. The TEM studies show that the Zn diffraction spots frequently correspond to the hexagonal structure, but NiO displays diffraction rings and spots consistent with its cubic structure. The energy band gap value of Zn: NiONC is 3.223 eV, according to the DRS spectra. The Congo Red (CR) dye photodegradation was used to assess the NC PCA. The results indicate that, under UV light irradiation, the highest absorption was seen at 497 nm with 80.9% degradation with respect to time. Zn: NiONC is also used as an electrode in CV studies. In a 1 M HCl solution, it shows the surface redox mechanism of Li to Li^+, which appeared at 0.31 V (cathodic) and 0.15 V (anodic) at 10 mV/s. By exhibiting a redox peak in the CV spectrum, the Zn: NiONC successfully identified lithium. This suggests that the electrode is suitable for use as a sensor electrode.

CONFLICT OF INTERESTS

The authors declare that there is no conflict of interest.

AUTHOR CONTRIBUTIONS

The present work is related to *SDG-7:Affordable and Clean Energy*. All the authors contributed significantly to this manuscript, participated in reviewing/editing and approved the final draft for publication. The research profile of the authors can be verified from their ORCID ids, given below:

Sharanakumar T.M. https://orcid.org/0000-0002-6427-9130
S.Soundeswaran https://orcid.org/0000-0002-2468-7746
G. Srinivas Reddy https://orcid.org/0000-0002-5651-986X
Puneeth Kumar N. https://orcid.org/0009-0001-1837-8955
T. Naveen Kumar https://orcid.org/0000-0002-0722-5216
K. M. Mamatha https://orcid.org/0009-0001-8972-2864
M.N. Somashekar https://orcid.org/0000-0002-9882-2920
C.R. Ravikumar https://orcid.org/0000-0002-4692-444X

Cite this article as: Sharanakumar T.M. *et al.*, *Rasayan J. Chem.*, 19(4), 2001-2013(2026), https://doi.org/10.31788/RJC.2026.1949958

REFERENCES

1. Z. Carmen, and S. Daniel, *Environmental and Analytical Update*, Book (2012), https://doi.org/10.5772/32373
2. S.D. Melvin, and F.D.L. Leusch, *Environment International*, **92–93** 183(2016), https://doi.org/10.1016/j.envint.2016.03.031
3. Z. Shan, Y. Yang, H. Shi, J. Zhu, X. Tan, Y. Luan, Z. Jiang, P. Wang, and J. Qin, *Frontiers in Chemistry,***9,** 755836(2021), https://doi.org/10.3389/fchem.2021.755836
4. M.H. Habibi, and E. Shojaee, *Spectrochimica Acta Part A: Molecular and Biomolecular Spectroscopy,* **229**, 117796(2020), https://doi.org/10.1016/j.saa.2019.117796
5. R. Ranjitha, K.N. Meghana, V.G.D. Kumar, A.S. Bhatt, B.K. Jayanna, C.R. Ravikumar, M.S. Santosh, H. Madhyastha, and K. Sakai, *New Journal of Chemistry,* **45,** 796(2021), https://doi.org/10.1039/D0NJ05268J
6. I. Rabani, C. Bathula, R. Zafar, G.Z. Rabani, S. Hussain, S.A. Patil, and Y.S. Seo, *Journal of Environmental Chemical Engineering,***9,** 104852(2021), https://doi.org/10.1016/j.jece.2020.104852

7. A. García-Rodríguez, V. Matamoros, C. Fontàs, and V. Salvadó, *Environmental Science and Pollution Research,* **21**, 11708(2014), https://doi.org/10.1007/s11356-013-2448-5
8. R. LakshmanaNaik, T. Bala Narsaiah, P. Justin, M. Dhanalakshmi, A. Naveen Kumar, M.N. Somashekar, T.M. Sharanakumar, C.R. Ravikumar, and H.C. Ananda Murthy, *Journal of the Indian Chemical Society,***101**, 101247(2024), https://doi.org/10.1016/j.jics.2024.101247
9. Arindam Dutta, Shirsendu Mitra, Mitali Basak, and Tamal Banerjee, *Energy Storage,* **5,** 1(2023), https://doi.org/10.1002/est2.339
10. Oluwaseye Samson Adedoja, Emmanuel Rotimi Sadiku, and Yskandar Hamam, *Polymers*, **15(10)**, 2272(2023), https://doi.org/10.3390/polym15102272
11. R.B. Rajput, S.N. Jamble, and R.B. Kale, *Journal of Environmental Management*, **307**, 114533(2022), https://doi.org/10.1016/j.jenvman.2022.114533
12. Rosana A. Gonçalves, Rosimara P. Toledo, Rosimara P. Toledo, Nirav Joshi, and Olivia M. Berengue, *Molecules*, **26(8)**, 2236(2021), https://doi.org/10.3390/molecules26082236
13. X. Liu, J. Iocozzia, Y. Wang, X. Cui, Y. Chen, S. Zhao, Z. Li, and Z. Lin, *Energy Environmental Science,* **10**, 402(2017), https://doi.org/10.1039/C6EE02265K
14. Aminuddin Bin Ahmad Kayani, Sruthi Kuriakose, Mahta Monshipouri, Fararishah Abdul Khalid, Sumeet Walia, Sharath Sriram, and Madhu Bhaskaran, *Nano Micro Small*, **17(32)**, 2100621(2021), https://doi.org/10.1002/smll.202100621
15. Noorah A. Al-Ahmadi, *Materials Research Express,***7,** 032001(2020), https://doi.org/10.1088/2053-1591/ab7a60
16. M.E. Khan, A. Mohammad, W. Ali, and A.A. Sharwani, *Inorganic Anticorrosive Materials*, **95–111**(2022), https://doi.org/10.1016/B978-0-323-90410-0.00006-4
17. A. Dey, *Materials Science and Engineering: B*, **229**, 206(2018), https://doi.org/10.1016/j.mseb.2017.12.036
18. U. Qumar, J.Z. Hassan, R.A. Bhatti, A. Raza, G. Nazir, W. Nabgan, and M. Ikram, *Journal of Materials Science & Technology*, **131**, 122(2022), https://doi.org/10.1016/j.jmst.2022.05.020
19. G. Nie, Y. Yao, X. Duan, L. Xiao, and S. Wang, *Current Opinion in Chemical Engineering,* **33** 100693(2021), https://doi.org/10.1016/j.coche.2021.100693
20. Ruibin Liang, Yongquan Du, Peng Xiao, Junyang Cheng, Shengjin Yuan, Yonglong Chen, Jian Yuan, and Jianwen Chen, *Nanomaterials*, **11(5)**, 1248(2021), https://doi.org/10.3390/nano11051248
21. X. Lin, L. Sheng, J. Yang, Y. Zhang, H. Shi, Y. Li, K. Wu, M. Han, X. Zhou, and L. Jiang, *Journal of Alloys and Compounds*, **990**, 174455(2024), https://doi.org/10.1016/j.jallcom.2024.174455
22. Gianluca Fiori, Francesco Bonaccorso, Giuseppe Iannaccone, Tomás Palacios, Daniel Neumaier, Alan Seabaugh, Sanjay K. Banerjee and Luigi Colombo. *Nature Nanotech*, **9**, 768(2014), https://doi.org/10.1038/nnano.2014.207
23. Yanchun Yang, Yinghui Han, Wenkun Jiang, Yuyang Zhang, Yanmei Xu, and Ayman Mahmoud Ahmed, *Applied Science*, **12(1)**, 354(2022), https://doi.org/10.3390/app12010354
24. P.C. Nagajyothi, S.V. Prabhakar Vattikuti, K.C. Devarayapalli, K. Yoo, J. Shim, and T.V.M. Sreekanth, *Critical Reviews in Environmental Science and Technology*, **50,** 2617(2020), https://doi.org/10.1080/10643389.2019.1705103
25. Maria P. Nikolova, Murthy S. Chavali, *Biomimetics*, **5(2),** 27(2020), https://doi.org/10.3390/biomimetics5020027
26. D. Kishore Kumar, J. Kříž, N. Bennett, B. Chen, H. Upadhayaya, K.R. Reddy, V. Sadhu, *Materials Science for Energy Technologies*, **3,** 472(2020), https://doi.org/10.1016/j.mset.2020.03.003
27. Maria P. Nikolova, and Murthy S. Chavali, *Biomimetics*, **5(2),** 27(2020), https://doi.org/10.3390/biomimetics5020027
28. N.R. Dhineshbabu, V. Rajendran, N. Nithyavathy and R. Vetumperumal, *Applied Nanoscience,* **6**, 933(2016), https://doi.org/10.1007/s13204-015-0499-2
29. M.S. Chavali, and M.P. Nikolova, *SN Applied Science,***1,** 607 (2019), https://doi.org/10.1007/s42452-019-0592-3
30. A.V. Nikam, B.L.V. Prasad, and A.A. Kulkarni, *CrystEngComm*, **20,** 5091(2018), https://doi.org/10.1039/C8CE00487K

31. M.R.A. Kumar, H.P. Nagaswarupa, C.R. Ravikumar, S.C. Prashantha, H. Nagabhushana, and A.S. Bhatt, *Journal of Physics and Chemistry of Solids*, **127**, 127(2019), https://doi.org/10.1016/j.jpcs.2018.12.012
32. D.J. Manasa, K.R. Chandrashekar, M.A. Pavan Kumar, D. Suresh, D.J. Madhu Kumar, C.R. Ravikumar, T. Bhattacharya, and H.C. Ananda Murthy, *Results in Chemistry*, **3**, 100178(2021), https://doi.org/10.1016/j.rechem.2021.100178
33. Alam, Mir Waqas, Muhammad Aamir, Mohd Farhan, Maryam Albuhulayqah, Mohamad M. Ahmad, C.R. Ravikumar, V.G. Dileep Kumar, and H.C. Ananda Murthy, *Crystals*, **11(12)**,1467(2021)., https://doi.org/10.3390/cryst11121467
34. R. Naik, A. Naveen Kumar, V. Shanbhag, C.R. Ravikumar, V. Revathi, N. Basavaraju, S.C. Prashantha, K.M. Girish, and H. Nagabhushana, *Inorganic Chemistry Communications*, **143**, 109760(2022), https://doi.org/10.1016/j.inoche.2022.109760
35. B. Abebe, D. Tsegaye, C. Sori, C.R. Ravikumar, and H.C.A. Murthy, *Optical Materials,***142**, 114072(2023), https://doi.org/10.1016/j.optmat.2023.114072
36. N. Nasir Ahamed, J. Pattar, M.R. Anil Kumar, N. Basavaraju, N. Raghavendra, S. T. M., C.R. Ravikumar, and H.C.A. Murthy, *RSC Advances,* **14**, 17664(2024), https://doi.org/10.1039/D4RA01706D
37. M.R.A. Kumar, C.R. Ravikumar, H.P. Nagaswarupa, B. Purshotam, B. Gonfa, H.C.A. Murthy, F.K. Sabir, and S. Tadesse, *Journal of Environmental Chemical Engineering,***7,** 103468(2019), https://doi.org/10.1016/j.jece.2019.103468
38. N. Nasir Ahamed, J. Pattar, V.G. Dileep Kumar, T. Naveen Kumar, N. Basavaraju, T.M. Sharanakumar, C.R. Ravikumar, *Analytical Chemistry Letters*, **14** 269(2024), https://doi.org/10.1080/22297928.2024.2361788
39. N. Afza, M.S. Shivakumar, M. Mylarappa, S.A. Subash, C.R. Ravikumar, T.M. Sharanakumar, and M.N. Somashekar, *Electrocatalysis,* **16**, 78 (2025), https://doi.org/10.1007/s12678-024-00898-3
40. Y.S. Nagaraju, H. Ganesh, S. Veeresh, H. Vijeth, M. Basappa, M. Vandana, and H. Devendrappa, *Materials Science in Semiconductor Processing*, **142,** 106429(2022), https://doi.org/10.1016/j.mssp.2021.106429
41. R.M. Obodo, A.C. Nwanya, M. Arshad, C. Iroegbu, I. Ahmad, R.U. Osuji, M. Maaza, and F.I. Ezema, *International Journal of Energy Research*, **44**, 3192(2020), https://doi.org/10.1002/er.5091
42. Y.S. Nagaraju, H. Ganesh, S. Veeresha, H. Vijeth, and H. Devendrappa, *Journal of Energy Storage*, **56**, 105924(2022), https://doi.org/10.1016/j.est.2022.105924
43. S. Saleem, M.N. Ashiq, S. Manzoor, U. Ali, R. Liaqat, A. Algahtani, S. Mujtaba, V. Tirth, A.M. Alsuhaibani, M.S. Refat, A. Ali, M. Aslam, and A. Zaman, *Journal of Materials Research and Technology*, **25**, 6150(2023), https://doi.org/10.1016/j.jmrt.2023.07.065
44. M.A.S. Amulya, H.P. Nagaswarupa, M.R.A. Kumar, C.R. Ravikumar, and K.B. Kusuma, *Journal of Physics and Chemistry of Solids,***148,** 109661(2021), https://doi.org/10.1016/j.jpcs.2020.109661
45. D.A. Raghupathy, G. Ramgopal, and C.R. Ravikumar, *Sensors International*, **3**, 100204(2022), https://doi.org/10.1016/j.sintl.2022.100204
46. N. Nasir Ahamed, J. Pattar, V.G. Dileep Kumar, T. Naveen Kumar, N. Basavaraju, T.M. Sharanakumar, and C.R. Ravikumar, *Analytical Chemistry Letters*, **14**, 269(2024), https://doi.org/10.1080/22297928.2024.2361788
47. U.S. Udayachandran Thampy, A. Mahesh, K.S. Sibi, I.N. Jawahar, and V. Biju, *SN Applied Science*. **1**,1478(2019), https://doi.org/10.1007/s42452-019-1426-z
48. D. Saravanakkumar, R. Karthika, S. Ganasaravanan, S. Sivaranjani, S. Pandiarajan, B. Ravikumar, and A. Ayeshamariam, *IOSR Journal of Applied Physics*, **10(3)**, 73(2018), https://doi.org/10.9790/4861-1003027383
49. S. Sivakumar, N.A. Mala, K.M. Batoo, and E.H. Raslan, *Materials Technology,* **37**, 1375(2022), https://doi.org/10.1080/10667857.2021.1949527
50. H.D. Weldekirstos, B. Habtewold, and D.M. Kabtamu, *Frontiers in Materials,* **9**, 832439(2022), https://doi.org/10.3389/fmats.2022.832439

51. Lakshmana Naik Ramavathu, T Bala Narsaiah, P Justin, Syed Khasim, A Naveen Kumar, N Raghavendra, R Ramesh and C R Ravikumar, *Material Research Express*, **10**, 125009(2023), https://doi.org/10.1088/2053-1591/ad184c
52. R. Lakshmana Naik, T. Bala Narsaiah, P. Justin, A. Naveen Kumar, M.N. Somashekar, N. Raghavendra, C.R. Ravikumar, A. Ahmad Khan, and M.S. Santosh, *Materials Science and Engineering: B*, **298**, 116861(2023), https://doi.org/10.1016/j.mseb.2023.116861
53. C. Valli Nachiyar, and G. Suseela Rajakumar, *Chemosphere,* **57**, 165(2004), https://doi.org/10.1016/j.chemosphere.2004.05.030
54. M.N. Sweilam, J.R. Varcoe, and C. Crean, *ACS Sensors,* **3(9)**, 1802(2018), https://doi.org/10.1021/acssensors.8b00528
55. F. Javanbakht, H. Najafi, K. Jalili, and M. Salami-Kalajahi, *Journal of Materials Chemistry A*, **11**, 26371(2023), https://doi.org/10.1039/D3TA06113B
56. I.A. Vitale, G. Selvolini, and G. Marrazza, *Chemosensors*, **11**, 77(2023), https://doi.org/10.3390/chemosensors11020077
57. M. Sheikh, M. Qassem, I.F. Triantis, and P.A. Kyriacou, *Sensors*, **22,** 736(2022), https://doi.org/10.3390/s22030736
58. K. Chetankumar, B.E.K. Swamy, and T.S.S.K. Naik, *Journal of Materials Science: Materials in Electronics*, **31**, 19728(2020), https://doi.org/10.1007/s10854-020-04498-x
59. J. Wang, J. Yang, P. Xu, H. Liu, L. Zhang, S. Zhang, and L. Tian, *Sensors and Actuators B: Chemical*, **306**, 127590(2020), https://doi.org/10.1016/j.snb.2019.127590

[RJC-9958/2026]